PAPER

ROYAL SOCIETY OF CHEMISTRY

Check for updates

First-principles calculations of inorganic metallocene nanowires†

Yangqi Ji,[a] Haifeng Lv [ID] *[ab] and Xiaojun Wu [ID] *[ab]

Inspired by the recently synthesized inorganic metallocene derivatives $Fe(P_4)_2^{2-}$, we have identified four stable inorganic metallocene nanowires, MP_4 (M = Sc, Ti, Cr and Fe) in configurations of either regular quadrangular prism (Q-type) or anticube (A-type), and further investigated their magnetic and electronic characteristics utilizing the first-principles calculation. It shows that CrP_4 is a ferromagnetic metal, while other nanowires are semiconducting antiferromagnets with bandgaps of 0.44, 1.88, and 2.29 eV within the HSE06 level. It also shows that both ScP_4 and TiP_4 can be stabilized in the Q-type and A-type, corresponding to the antiferromagnetic and ferromagnetic ground states, respectively, indicating a configuration-dependent magnetism. The thermodynamic and lattice stabilities are confirmed by the *ab initio* molecular dynamics and phonon spectra. This study has unmasked the structural and physical properties of novel inorganic metallocene nanowires, and revealed their potential application in spintronics.

Introduction

Since the milestone discovery of ferrocene,[1] the multidecker molecular complexes in the form of sandwich clusters and their infinitely extended nanowires have attracted great research interest due to the distinct structural, optical,[2,3] chemical,[4] electrical,[5] and magnetic properties,[6] rendering them potential candidates in catalysis,[7] electronics and spintronics.[8–12] Especially, the tunable coordination mode between the central metal and organic molecules accompanied by diverse charge transfer and crystal field splitting can lead to unpaired d electrons and form intriguing magnetic ordering phenomena.[13–15] For instance, the organometallic complexes composed of vanadium and benzene, $V_n(Bz)_m$ (Bz = C_6H_6), were confirmed to be molecular magnets and the magnetic moments of the complexes increase with the central metal atoms.[16,17] Then, theoretical study revealed that the one-dimensional $[V(Bz)]_\infty$ and $[Mn(Bz)]_\infty$ are quasi- or half-metallic.[18] Also, $(VCp)_\infty$ (Cp = C_5H_5), $(VBzVCp)_\infty$, and $(V_2Ant)_\infty$ wires (Ant = anthracene) are ferromagnetic half-metals.[19] Based on pentalene (Pn = C_8H_6), double metallocene nanowires were predicted, in which the $PnMn_2$ nanowire exhibits ferromagnetic behavior.[20] Among the homo-bimetallic naphthalene (Np=$C_{10}H_8$), namely $NpTM_2$,

(TM = V, Mn, Ti, Nb) nanowires, $NpMn_2$ is ferromagnetic, $NpTi_2$ and $NpNb_2$ are antiferromagnetic, and NpV_2 exhibits carrier-tunable magnetic ordering.[21] Then, the hetero-bimetallic naphthalene nanowires, $[Np_2V_2Cr_2]_\infty$, $[Np_2V_2Mn_2]_\infty$, and $[Np_2V_2Fe_2]_\infty$ are shown as half-metals, while $[Np_2V_2Cr_2]_\infty$ is quasi-half-metallic,[22] and the $V_{n-1}Np_n$ nanowire also exhibits carrier-tunable magnetic ordering.[23] Theoretical studies also demonstrated that the sandwiched Eu_nCOT_{n+1} (Eu = europium, COT = C_8H_8, n = 1–4) clusters are molecular magnets.[24] By using the chemical functionalization, the multiferroic organometallic molecular nanowires were predicted.[25] A recent study showed that ferromagnetic half-metallicity can be realized in metal tri-hydride molecular nanowires.[15] As a result, exploring novel metallocene-analogue molecular clusters and nanowires with magnetism is highly desirable due to their high potential application as one-dimensional spintronics.

To enrich the family of multidecker sandwich complexes, great efforts have been made to explore molecules similar to ferrocene and it is assumed that a heteroelement derivative can be obtained by the isolobal replacement of CH with group 15 phosphorus, which may possess distinct properties with various bond types and coordination environment.[26] Despite the high stability of $Fe(\eta^5\text{-}P_5)_2$ confirmed by the theoretical calculation,[27] experimental realization has not been achieved, and only a molecular complex $Ti(\eta^5\text{-}P_5)_2$ was reported to be synthesized so far.[28] Cyclo-P_4, which can accommodate two electrons, is believed to be more useful in contrast to the monoanionic cyclo-P_5.[29] Very recently, Wang *et al.* has synthesized a ferrocene derivative $[Fe(P_4)_2]^{2-}$ by using Zintl ions as precursors,[30] which may serve as the building block for the inorganic metallocene complexes.

Enlighted by the recently synthesized $Fe(P_4)_2^{2-}$, inorganic metallocene nanowires, MP_4 (M = Sc, Ti, Cr and Fe) are reported

[a]School of Chemistry and Materials Science, CAS Key Laboratory of Materials for Energy Conversion, CAS Center for Excellence in Nanoscience, University of Science and Technology of China, Hefei, Anhui 230026, China

[b]Key Laboratory of Precision and Intelligent Chemistry, University of Science and Technology of China, Hefei, Anhui 230026, China. E-mail: xjwu@ustc.edu.cn

and the structural, electrical, and magnetic characteristics are investigated within the first-principles calculation. Our results show that ScP_4, TiP_4, CrP_4 and FeP_4 can form stable one-dimensional nanowires in either regular quadrangular prism (Q-type) or anticube (A-type) configurations. Among them, ScP_4, TiP_4 and FeP_4 nanowires have antiferromagnetic (AFM) ground state and CrP_4 nanowires are ferromagnetic (FM). AIMD simulation and phonon spectrum calculations have confirmed their thermodynamic and lattice stabilities.

Methods

First-principles calculations were performed by using the Perdew–Burke–Ernzerhof (PBE) functional and Projector Augmented Wave (PAW) potential within the Vienna *ab initio* simulation (VASP) package.[31–35] A cut-off energy of 400 eV was adopted, and the atomic positions and lattice constant along the extended direction were relaxed until the force and energy were smaller than 0.01 eV Å^{-1} and 1×10^{-5} eV. A Γ-centered $1 \times 1 \times 8$ k-points was used. According to the previous research,[36,37] a Hubbard U_{eff} value of 3 eV was adopted to account for the strong correlation effect. To obtain a more accurate electronic structure, the Heyd–Scuseria–Ernzerhof hybrid functional (HSE06) was adopted.[38] One-dimensional chains were chosen to extend along the c-axis, while a certain vacuum layer thickness (around 10 Å) is added in the other directions of the unit cell to avoid repetitive disturbances of the force field under the periodic boundary conditions. Considering the van der Waals (vdW) interactions, the Grimme DFT-D3 correction was utilized.[39] Additionally, *ab initio* molecular dynamics (AIMD) simulations were executed with the supercell of $1 \times 1 \times 4$ and the total time was 5 ps with each step of 1 fs, using the *NVT* ensemble. The phonon spectra were calculated with density-functional-perturbation theory (DFPT) using PHONOPY.[40] The post-processing calculations for the relevant calculations were performed using the VESTA software[41] and VASPKIT code.[42]

Results and discussion

According to Fig. 1(a), the MP_4 molecular complex is composed of one transition metal atom sandwiched between two square cyclo-P_4 rings, owning to the C_{4v} symmetry and forming an $\eta^4 : \eta^4$ coordination pattern. The P_4 rings can arrange into two configurations, namely, regular quadrangular prism (Q-type) (Fig. 1(b)) or anticube (A-type) (Fig. 1(c)). Hence, two types of MP_4 nanowires are considered, as shown in Fig. 1(d) and (e), respectively. Then, the geometrical configurations of MP_4 nanowires (M = Sc to Ni) in Q-type and A-type are relaxed and it shows that ScP_4, CrP_4, and FeP_4 are energetically more stable in the Q-type and TiP_4 is energetically more stable in the A-type, as displayed in Table S1.† Cu and Zn are excluded due to their absence of metallocene forms. The lattice stability of the energetically stable MP_4 is identified according to their phonon spectra. As displayed in Fig. S1,† imaginary frequencies are absent for the ScP_4, CrP_4, and FeP_4, and a small imaginary frequency in TiP_4 nanowires is partly attributed to the flat potential energy surface at its ground state. Hence, the
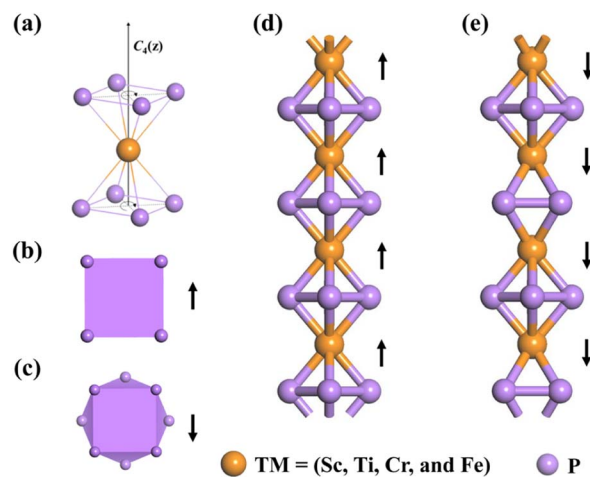

Fig. 1 Models of (a) MP_4 molecular complex, (b) regular quadrangular prism (Q-type) ligand field, (c) anticube (A-type) ligand field, (d) Q-type MP_4 nanowire, and (e) A-type MP_4 nanowire. The "up" and "down" arrows indicate the different stacking models of cyclo-P_4 rings.

calculations below are based on the ScP_4, TiP_4, CrP_4 and FeP_4 nanowires.

As demonstrated in Table 1, the M–P distances exhibit a range of 2.46 to 2.70 Å, descending from Sc to Fe, and the P–P distances among adjacent P atoms vary from 2.24 to 2.28 Å, indicating the elongated P–P distance compared to black phosphorus (2.18 Å).[43] To further determine their stability, we calculated the averaged formation energy per unit cell, which is described as below, in which $E_{NW}[MP_4]$, $E[M]$, and $E[P_4]$ are the energies of the nanowire, single metal atom, and cyclo-P_4 ring, respectively.

$$E_f[MP_4] = E_{NW}[MP_4] - E[M] - E[P_4]$$

The calculated formation energies vary from -5.79 to -8.00 eV, in which the negative formation energies indicate that the formation of MP_4 nanowires from the P_4 ring and metal atom is exothermic, and ScP_4 nanowire has the largest formation energy. These values are larger or comparable to those for other organic multidecker nanowires, including transition

Table 1 Metal–phosphorus bond distance (d_{MP}, Å), phosphorus–phosphorus bond distance (d_{PP}, Å), averaged formation energy per unit cell (E_f, eV), transferred charge from the metal to phosphorus (C, e), and atomic magnetic moment (M, μB) on each metal atom, ground state (GS, in which S and M denote the semiconductor and metal), and energy difference ($\Delta E = E(FM) - E(AFM)$, eV) between ferromagnetic (FM) and antiferromagnetic (AFM) states per unit cell

	ScP_4	TiP_4	CrP_4	FeP_4
d_{MP}	2.70	2.55	2.52	2.46
d_{PP}	2.26	2.28	2.24	2.24
E_f	-8.00	-7.99	-5.79	-6.43
C	1.67	1.55	1.01	0.76
M	0.16	0.80	3.31	3.21
GS	AFM S	AFM S	FM M	AFM S
ΔE	0.02	0.68	-0.58	0.66

metal benzene nanowires (−1.71 to −5.33 eV) or metallocene nanowires.[18,44]

In addition, we also examined the thermodynamic stability of the MP_4 nanowires by conducting the *ab initio* molecular dynamics (AIMD) simulation at temperatures increasing up to 700 K. The evolution of total energy and magnetic moments along with time, and the last snapshots for the AIMD simulations are shown in Fig. S4.† It can be observed that the structural motif A-type TiP_4 nanowires can be maintained at 300 K. CrP_4 nanowires are able to maintain their structure at 400 K, FeP_4 at 500 K, and for ScP_4, the temperature can reach up to 700 K. The difference in thermodynamic stability can be elucidated by the energy difference between the A-type and the Q-type structures in the same magnetic ground state per unit cell, as shown in Table S1.† The energy difference between the Q-type and A-type CrP_4 nanowires in the FM state is the smallest (0.196 eV), and ScP_4 has the largest energy difference (0.759 eV), leading to different thermodynamic stabilities. Meanwhile, the poor thermodynamic stability of TiP_4 is partly attributed to the low oxidation state of central Ti.

Next, the magnetic ground states of the MP_4 nanowires are confirmed and three magnetic states are considered, ferromagnetic (FM), antiferromagnetic (AFM) states, and nonmagnetic states (NM). The ScP_4, TiP_4 and FeP_4 nanowires are identified to be antiferromagnetic, in which the energy differences are 0.02 eV, 0.68 eV and 0.66 eV between the FM and AFM states. Particularly, the CrP_4 nanowires are ferromagnetic in their ground state, which is 0.58 eV energetically lower than the AFM state. The atomic magnetic moments of Sc, Ti, Cr, and Fe atoms are 0.16, 0.80, 3.31, and 3.21 μB, respectively. We have provided the element-resolved density of states and the spatial distribution of CBM/VBM decomposed charge density in the real space for the three semiconducting nanowires at the same isosurface level in Fig. S5 and S9.† It shows that for ScP_4 (Fig. S9(a and b)†) the VBM and CBM are contributed by $d_{xy}/d_{x^2-y^2}$, for TiP_4 (Fig. S9(c and d)†) the VBM and CBM are contributed by $d_{xy}/d_{x^2-y^2}$ and d_{z^2}, respectively, for FeP_4 (Fig. S9(e and f)†) the VBM and CBM are contributed by d_{xz}/d_{yz} and d_{z^2}, respectively, which is well-accorded with the calculated electronic structures in Fig. 2 and S6.†

Then, the band structures of the MP_4 nanowires are illustrated in Fig. 2. ScP_4 and FeP_4 nanowires have direct band gaps with bandgaps of 0.44 eV and 2.29 eV, and the TiP_4 nanowires have an indirect bandgap with bandgaps of 1.88 eV at the HSE06 level, respectively. Meanwhile, CrP_4 nanowires are metallic.

Next, we have tried to understand the origin of magnetism of the MP_4 nanowires. In a regular quadrangular prism crystal field, five 3d orbitals of metal atoms are readily split into a doubly degenerate band e (d_{xz}, d_{yz}), and three singly degenerate bands a_1, a_2, a_3 (d_{xy}, $d_{x^2-y^2}$, and d_{z^2}) for the MP_4 nanowire except for CrP_4. For CrP_4, the residual unpaired electrons can fill one of the doubly degenerate orbitals and the other is empty, resulting in five single d orbitals. In anticube configurations, five 3d orbitals of metal atoms can be split into doubly degenerate bands e1(d_{xy}, $d_{x^2-y^2}$), e2(d_{xz}, d_{yz}), and a singly degenerate band a(d_{z^2}). Their density of states is shown in Fig. S5.† It also shows that the direction of electron transfer is from the metal
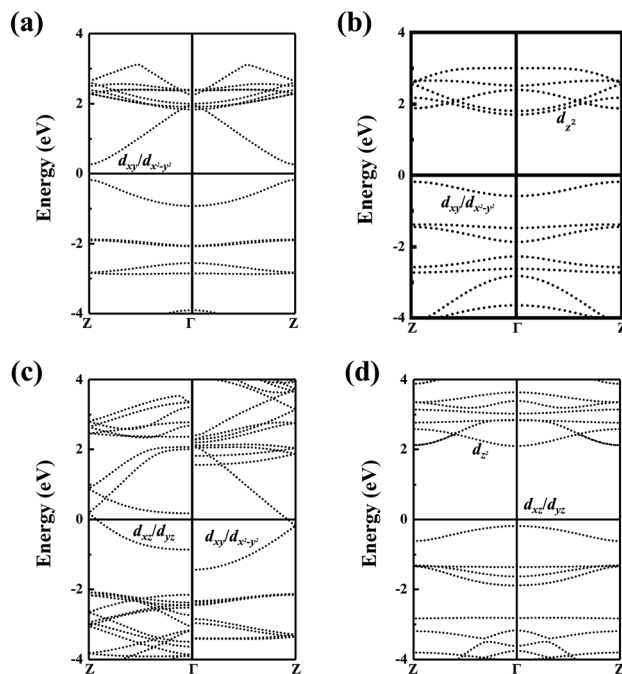

Fig. 2 The electronic band structures for (a) ScP_4, (b) TiP_4, (c) CrP_4, and (d) FeP_4 nanowires at the HSE06 level.

atom to the P_4 ring using the Bader charge analysis (Table 1), and residual unpaired d electrons account for the existence of magnetism.

Furthermore, we have plotted the electronic configuration of metal atoms to understand the diverse magnetic ground states in CrP_4 and FeP_4 nanowires. Based on the crystal field splitting theory and Bader charge analysis, the electronic configuration of metal ions in CrP_4 and FeP_4 nanowires are shown in Fig. S10.† As shown, both Cr and Fe ions have half-filled orbitals and the cation–anion–cation bond angle is 180°. According to the super exchange interaction theory,[45] two magnetic ions with half-occupied orbitals coupled through an intermediary nonmagnetic ion lead to a strong anti-ferromagnetic coupling, which confirmed the antiferromagnetic coupling in FeP_4 nanowires (Fig. S10(a)†). However, for CrP_4, the P_4 ring is slightly magnetized according to the spin charge density (Fig. S8(c)†), leading to the spin exchange pathway in Fig. S10(b)† and ferromagnetic coupling between Cr ions.

Considering the rotation of P_4 rings, we have also investigated the meta-stable phase of MP_4 nanowires and it shows that ScP_4 and TiP_4 can be stabilized in both regular quadrangular prism (Q-type) and anticube (A-type) configurations (Fig. S3†), corresponding to AFM and FM ground states, respectively, indicating a novel configuration-dependent magnetism. According to their electronic band structures (Fig. S7†), ScP_4 is a BMS (Bipolar Magnetic Semiconductor)[46] material of A-type and TiP_4 is a ferromagnetic metal of Q-type, showing a configuration tunable magnetism.

Based on the Mermin–Wagner theorem,[47] long-range magnetic order is absent for any infinitely strict one-dimensional isotropic system at non-zero temperature.

However, the relatively large magnetic crystalline anisotropic energy can help to hinder thermal fluctuation and stabilize the long-range ordering in one-dimensional or quasi-one-dimensional systems.[48] Then, non-collinear calculations are conducted and the results in Table S2† show that easy-axis of MP_4 (M = Sc, Ti, Cr, Fe) is normal to the nanowires and the magnetic anisotropic energy values are 0.18, 13.58, 77.86, and 326.18 μeV per atom. TiP_4, CrP_4 and FeP_4 are higher or comparable to the bulk b.c.c.Fe (−1.4 μeV per atom), bulk h.c.p.Co (−65 μeV per atom), bulk f.c.c.Co (1.8 μeV per atom), and bulk f.c.c.Ni (2.7 μeV per atom),[49,50] suggesting the possibility of maintaining the long-range magnetic ordering. Also, the long-range magnetic order can be stabilized by the interchain coupling of MP_4 nanowires. Then, we calculated the inter-chain coupling between two CrP_4 nanowires with an optimized distance of about 3.8 Å (Fig. S11†). It was found that the inter-chain magnetic coupling is FM, which is 0.72 meV M^{-1} lower than AFM coupling in energy with a J value of 0.26 meV. This value is relatively larger than that of p-nitrophenyl nitro-oxide (p-NPNN), which exhibits a Curie temperature of 0.65 K and the interchain coupling J is estimated to be about 0.1 K (0.009 meV).[51]

Conclusions

In summary, this work reports four types of MP_4 inorganic metallocene nanowires (M = Sc, Cr, Ti, Fe) that exhibit different electronic and magnetic properties. Our calculations show that MP_4 clusters can form stable one-dimensional nanowires. ScP_4, TiP_4 and FeP_4 nanowires are AFM semiconductors, while CrP_4 is an FM metal in the ground state. Phonon spectrum calculations and AIMD simulations demonstrate the lattice and thermodynamic stability of these nanowires. The formation of MP_4 nanowires *via* assembly of the P_4 ring and metal atoms is exothermic. Both ScP_4 and TiP_4 can be stabilized in the Q-type and A-type, corresponding to AFM and FM ground states, respectively, suggesting a novel configuration-dependent magnetism. These results reveal the potential application of MP_4 nanowires in spintronics. This work can promote the development of one-dimensional spintronics based on the inorganic molecular complexes.

Author contributions

X. W. and H. L. designed the project. Y. J. and H. L. performed the calculation and analysed the data. Y. J., H. L., and X. W. wrote the manuscript.

Conflicts of interest

There are no conflicts to declare.

Acknowledgements

References

1 T. J. Kealy and P. L. Pauson, *Nature*, 1951, **168**, 1039–1040.

2 S.-J. Wang, Y.-F. Wang and C. Cai, *J. Phys. Chem. C*, 2015, **119**, 16256–16262.

3 S.-J. Wang, Y. Li, D. Wu, Y.-F. Wang and Z.-R. Li, *J. Phys. Chem. A*, 2012, **116**, 9189–9196.

4 X. Liu, Y. Tan, Z. Ma and Y. Pei, *J. Phys. Chem. C*, 2016, **120**, 27980–27988.

5 N. Hosoya, R. Takegami, J.-I. Suzumura, K. Yada, K. Miyajima, M. Mitsui, M. B. Knickelbein, S. Yabushita and A. Nakajima, *J. Phys. Chem. A*, 2014, **118**, 8298–8308.

6 T. Xie and W. Qin, *J. Phys. Chem. C*, 2016, **120**, 24498–24502.

7 L. Münzfeld, S. Gillhuber, A. Hauser, S. Lebedkin, P. Hädinger, N. D. Knöfel, C. Zovko, M. T. Gamer, F. Weigend, M. M. Kappes and P. W. Roesky, *Nature*, 2023, **620**, 92–96.

8 J. L. Wang, X. Y. Zhang, P. V. R. Schleyer and Z. F. Chen, *J. Chem. Phys.*, 2008, **128**, 104706.

9 Y. X. Wang, C. C. Sun, Z. D. Yang, H. Yu, P. Pan, L. Pei, G. L. Zhang and Y. Y. Hu, *Chem. Phys.*, 2019, **523**, 1–6.

10 X. Liu, Y. Tan, G. Zhang and Y. Pei, *J. Phys. Chem. C*, 2018, **122**, 16168–16177.

11 Z. Yang, B. L. Zhang, X. G. Liu, Y. Z. Yang, X. Y. Li, S. J. Xiong and B. S. Xu, *Org. Electron.*, 2013, **14**, 2916–2924.

12 P. Gain, R. Jana and A. Datta, *J. Phys. Chem. A*, 2021, **125**, 3362–3368.

13 L. Zhou, S.-W. Yang, M.-F. Ng, M. B. Sullivan, V. B. C. Tan and L. Shen, *J. Am. Chem. Soc.*, 2008, **130**, 4023–4027.

14 L. Wang, X. Gao, X. Yan, J. Zhou, Z. Gao, S. Nagase, S. Sanvito, Y. Maeda, T. Akasaka, W. N. Mei and J. Lu, *J. Phys. Chem. C*, 2010, **114**, 21893–21899.

15 X. Li, H. Lv, J. Dai, L. Ma, X. C. Zeng, X. Wu and J. Yang, *J. Am. Chem. Soc.*, 2017, **139**, 6290–6293.

16 K. Miyajima, A. Nakajima, S. Yabushita, M. B. Knickelbein and K. Kaya, *J. Am. Chem. Soc.*, 2004, **126**, 13202–13203.

17 J. Wang, P. H. Acioli and J. Jellinek, *J. Am. Chem. Soc.*, 2005, **127**, 2812–2813.

18 H. Xiang, J. Yang, J. G. Hou and Q. Zhu, *J. Am. Chem. Soc.*, 2006, **128**, 2310–2314.

19 L. Wang, Z. Cai, J. Wang, J. Lu, G. Luo, L. Lai, J. Zhou, R. Qin, Z. Gao, D. Yu, G. Li, W. N. Mei and S. Sanvito, *Nano Lett.*, 2008, **8**, 3640–3644.

20 X. Wu and X. C. Zeng, *J. Am. Chem. Soc.*, 2009, **131**, 14246–14248.

21 Z. Zhang, X. Wu, W. Guo and X. C. Zeng, *J. Am. Chem. Soc.*, 2010, **132**, 10215–10217.

22 X. Zhang, J. Han, Y. Liu and J. Wang, *J. Phys. Chem. C*, 2012, **116**, 5414–5419.

23 Y. Li, Z. Zhou and Z. Chen, *J. Phys. Chem. A*, 2012, **116**, 1648–1654.

24 X. Zhang, M.-F. Ng, Y. Wang, J. Wang and S.-W. Yang, *ACS Nano*, 2009, **3**, 2515–2522.

25 M. Wu, J. D. Burton, E. Y. Tsymbal, X. C. Zeng and P. Jena, *J. Am. Chem. Soc.*, 2012, **134**, 14423–14429.

26 N. Kuhn, E.-M. Horn, R. Boese and N. Augart, *Angew Chem. Int. Ed. Engl.*, 1988, **27**, 1368–1369.

27 G. Frenking, K. Wichmann, N. Fröhlich, C. Loschen, M. Lein, J. Frunzke and V. M. Rayón, *Coord. Chem. Rev.*, 2003, **238**, 55–82.

28 E. Urnezius, W. W. Brennessel, C. J. Cramer, J. E. Ellis and P. V. Schleyer, *Science*, 2002, **295**, 832–834.

29 J. Trygg, B. Johansson, O. Eriksson and J. M. Wills, *Phys. Rev. Lett.*, 1995, **75**, 2871–2874.

30 Z.-C. Wang, L. Qiao, Z.-M. Sun and M. Scheer, *J. Am. Chem. Soc.*, 2022, **144**, 6698–6702.

31 G. Kresse and J. Furthmuller, *Phys. Rev. B: Condens. Matter Mater. Phys.*, 1996, **54**, 11169–11186.

32 G. Kresse and J. Furthmuller, *Comput. Mater. Sci.*, 1996, **6**, 15–50.

33 J. P. Perdew, K. Burke and M. Ernzerhof, *Phys. Rev. Lett.*, 1996, **77**, 3865–3868.

34 P. E. Blöchl, *Phys. Rev. B: Condens. Matter Mater. Phys.*, 1994, **50**, 17953–17979.

35 G. Kresse and D. Joubert, *Phys. Rev. B: Condens. Matter Mater. Phys.*, 1999, **59**, 1758–1775.

36 Y. G. Zhang, Z. Cui, B. S. Sa, N. H. Miao, J. Zhou and Z. M. Sun, *Nanoscale Horiz.*, 2022, **7**, 276–287.

37 S. Y. Wang, N. X. Miao, K. H. Su, V. A. Blatov and J. J. Wang, *Nanoscale*, 2021, **13**, 8254–8263.

38 J. Heyd, G. E. Scuseria and M. Ernzerhof, *J. Chem. Phys.*, 2006, **124**, 219906.

39 S. Grimme, *J. Comput. Chem.*, 2006, **27**, 1787–1799.

40 A. Togo and I. Tanaka, *Scr. Mater.*, 2015, **108**, 1–5.

41 K. Momma and F. Izumi, *J. Appl. Crystallogr.*, 2011, **44**, 1272–1276.

42 V. Wang, N. Xu, J. C. Liu, G. Tang and W. T. Geng, *Comput. Phys. Commun.*, 2021, **267**, 108033.

43 P. Chen, N. Li, X. Chen, W.-J. Ong and X. Zhao, *2D Mater.*, 2017, **5**, 014002.

44 L. Shen, S. W. Yang, M. F. Ng, V. Ligatchev, L. P. Zhou and Y. P. Feng, *J. Am. Chem. Soc.*, 2008, **130**, 13956–13960.

45 J. B. Goodenough, *Magnetism and the Chemical Bond*, Wiley-Interscience, New-York, 1963.

46 H. D. Wang, Q. Q. Feng, X. X. Li and J. L. Yang, *Research*, 2022, 9857631.

47 N. D. Mermin and H. Wagner, *Phys. Rev. Lett.*, 1966, **17**, 1133–1136.

48 P. Gambardella, A. Dallmeyer, K. Maiti, M. C. Malagoli, W. Eberhardt, K. Kern and C. Carbone, *Nature*, 2002, **416**, 301–304.

49 A. N. Anisimov, M. Farle, P. Poulopoulos, W. Platow, K. Baberschke, P. Isberg, R. Wäppling, A. M. N. Niklasson and O. Eriksson, *Phys. Rev. Lett.*, 1999, **82**, 2390–2393.

50 J. Trygg, B. Johansson, O. Eriksson and J. M. Wills, *Phys. Rev. Lett.*, 1995, **75**, 2871–2874.

51 M. Takahashi, P. Turek, Y. Nakazawa, M. Tamura, K. Nozawa, D. Shiomi, M. Ishikawa and M. Kinoshita, *Phys. Rev. Lett.*, 1991, **67**, 746–748.